Thesis for The Degree of Licentiate of Philosophy

Modelling and Linking Radar Backscatter and Stem Water Content in a Boreal Forest

Theresa Leistner

Department of Space, Earth and Environment
Chalmers University of Technology
Gothenburg, Sweden, 2025

Modelling and Linking Radar Backscatter and Stem Water Content in a Boreal Forest

Theresa Leistner

Department of Space, Earth and Environment
Division of Geoscience and Remote Sensing
Chalmers University of Technology
SE-412 96 Gothenburg,
Sweden
Phone: +46(0)31 772 1000

Cover: The boreal forest observed by the BorealScat-2 radar tower, seen in the background. Photo: Patrik Bennet.

Printed by Chalmers Digitaltryck,
Gothenburg, Sweden 2025.

Modelling and Linking Radar Backscatter and Stem Water Content in a Boreal Forest

Theresa Leistner

Department of Space, Earth and Environment
Chalmers University of Technology

Abstract

In the context of climate change, forests serve as crucial mitigators but are also increasingly threatened by disturbances such as wildfires, insect outbreaks, and windthrows. Monitoring forest vitality is essential, with tree water status serving as an important indicator of forest health.

Spaceborne synthetic aperture radar (SAR), known for its sensitivity to vegetation water content (VWC), offers a promising tool for providing forest VWC on a global scale with high spatial resolution. However, the processes linking SAR backscatter to forest VWC are not fully understood. This thesis addresses this gap by establishing a link between radar backscatter and stem water content in boreal forests, using data from two tower-based radars, BorealScat and BorealScat-2, as an intermediary platform.

In Paper I, for the first time, the relevance of tower-based radar observations for spaceborne SAR was examined. This was done by comparison of time series of BorealScat radar backscatter and backscatter observed by Sentinel-1 and ALOS-2 PALSAR-2 at C- and L-band, respectively. A good agreement was found for a healthy forest, with an RMSE of 0.9 dB and 0.6 dB at C-band and L-band, respectively. At C-band, tree death was visible in tomographic tower-based backscatter but not in Sentinel-1 or BorealScat full-forest backscatter, indicating the potential value of tomographic spaceborne SAR missions for forest vitality monitoring.

In Paper II, for the first time, forest backscatter was linked to high quality stem water content measurements. A modified version of the water cloud model was used to relate stem water content time series to canopy backscatter and attenuation time series observed at L-band by BorealScat-2. Modelled stem water content closely matched in situ stem water content with a relative RMSE of 4% and 2% for the inversion of the canopy backscatter model and the inversion of the attenuation model, respectively. These findings demonstrate the feasibility of using L-band SAR backscatter to monitor VWC and the value of tomography in future spaceborne SAR missions.

Keywords

Remote sensing, synthetic aperture radar, forest, vegetation water content, L-band, C-band, stem water content, tomography

List of Publications

Appended papers

This thesis is based on the following publications:

[**Paper I**] **T. Leistner**, A. R. Monteith, L. M. H. Ulander, *"Comparison of Tower-Based and Satellite L- and C-Band Radar Backscatter from a Boreal Forest".*
IGARSS 2023 - 2023 IEEE International Geoscience and Remote Sensing Symposium, Pasadena, CA, USA, 2023, pp. 8319-8322. doi: 10.1109/IGARSS52108.2023.10283155.

[**Paper II**] **T. Leistner**, A. R. Monteith, J. Gutierrez Lopez, L. M. H. Ulander, *"Estimation of Stem Water Content from Tower-Based L-Band Radar Backscatter of a Boreal Forest".*
Submitted manuscript.

Other papers

The author has contributed to the following paper that is related to the work in this thesis, but is not appended.

[**a**] A. R. Monteith, L. M. H. Ulander, S. C. Steele-Dunne, P. J. Bennet, J. Westin, H. J. Persson, **T. Leistner**, H. Laudon, J. E. S. Fransson, *"A Tower-Based Radar Experiment for Studying the Effects of Boreal Forest Tree-Water Relations".*
Under review.

Acknowledgements

First and foremost, I would like to thank my supervisor, Lars Ulander, for giving me the opportunity to undertake this work and for his guidance and support. I appreciate his commitment to scientific accuracy, which has strengthened my belief in the importance of rigorous research.

I would also like to thank my assistant supervisor, Albert Monteith, for his encouragement and for always taking the time to discuss both smaller and larger questions. This truly helped me balance my work priorities.

Also thanks to my assistant supervisors Johan Fransson, Torgny Näsholm and my examinator Patrick Eriksson for their feedback on this thesis, and our collaborators at SLU for helping to make this work possible.

Thanks to my colleagues at the Division of Geoscience and Remote Sensing for creating a pleasant work environment through both work-related and casual discussions.

Finally, I thank Felix for moving with me to Gothenburg and for always being there for me. I very much enjoy our life together with Stellan.

Contents

Part I

Summary

Chapter 1

Introduction

Forests are an important component of the Earth's biosphere, playing a critical role in regulating the Earth's climate [1], weather patterns and ecosystems. They mostly act as carbon sinks, absorbing vast amounts of atmospheric CO_2 [2], and provide habitats for countless species, thereby sustaining global biodiversity [3]. Forests also influence local and regional climates by modulating temperature, humidity, and precipitation.

Healthy forests mitigate climate change by acting as carbon sinks and contributing to a net cooling effect through evapotranspiration (ET) [4]. However, climate change itself poses severe threats to forest vitality, with disturbances like wildfires, droughts, insect outbreaks and windthrows expected to become more frequent and severe [5].

Monitoring forest vitality and understanding forests' roles in the Earth's hydrological cycle and climate are urgently needed. Vegetation water content (VWC) is a critical indicator of forest health, reflecting the tree's physiological state and responses to environmental stress [6], [7]. Moreover, continuous monitoring of this variable helps quantify the role forests play in the Earth's hydrological cycle and their impact on the climate. Despite its importance, no existing method can provide reliable large-scale measurements of VWC in forests. Nevertheless, effective monitoring of forest health and their roles in the hydrological and carbon cycles on a global scale is only feasible through spaceborne platforms [8].

Passive microwave remote sensing can be used to estimate vegetation optical depth [9], [10], which is often assumed to be linearly related to VWC. However, most passive remote sensing sensors have a relatively coarse resolution, which limits their applicability, particularly for heterogeneous forest landscapes.

Airborne lidar, operating at optical frequencies, is one of the most accurate remote sensing methods for forest structure and above-ground biomass mapping [11]. However, lidar is not directly sensitive to water stored within tree structures and its application is limited by cloud cover. Additionally, spaceborne applications of this technique face challenges due to unresolved issues related to resolution, coverage, and technological constraints [12]. In contrast, microwaves can penetrate vegetation canopies, operate under all weather conditions, and

are directly sensitive to water content within tree structures, making them useful for monitoring VWC.

Spaceborne synthetic aperture radar (SAR) operates at microwave frequencies and can provide regional and global spatial coverage together with fine spatial resolution. In addition, SAR has the potential of using tomography which allows to separate contributions of different height layers [13].

The objective of this thesis is to understand the link between satellite SAR data and VWC in forests. This link is not investigated directly but indirectly by the use of the BorealScat radar towers [14]–[16]. In the first appended paper, the relevance of the tower observations for spaceborne SAR missions is established at two frequency bands, C-band and L-band (Paper I). In the second appended paper, tower-based observations at L-band are linked to the VWC of a forest by introducing a model, that relates backscatter to stem water content (Paper II).

Chapter 2 will briefly explain water movement within the forest and how tree water variables can be measured and modelled. Chapter 3 will then introduce the measurement techniques used in this thesis, radar remote sensing and discuss modelling of forest backscatter. Summaries of the appended papers are given in Chapter 4. Future work is discussed in Chapter 5. Part II consists of the appended papers to this thesis.

Chapter 2

Tree Water Dynamics

2.1 The Soil-Plant-Atmosphere Continuum

All trees require photosynthesis to sustain their life and growth. One consequence of photosynthesis is transpiration, which is the loss of water via leaf pores, known as stomata, to the atmosphere. Water transport from the soil to the leaves occurs within the xylem tissue, which for conifers consists of tracheids, which are pipe-like structures located in the roots, stem and branches of the tree. The xylem tissue is surrounded by the cambium, and outside the cambium is the phloem tissue, which consists of living, elastic cells that have some water storage capacity[17].

Upward transport of water within trees occurs along the negative gradient of water potential [18]. Water potential is a measure of the potential energy of water in a system compared to pure water at a reference temperature and pressure. The gradient of water potential determines the direction in which water will move. Water potential generally consists of an osmotic component due to the presence of solutes, a hydrostatic component due to physical pressure in the system, a gravitational component and a matrix component due to the adhesion of water molecules to surfaces. The movement of water along the soil-plant-atmosphere continuum (SPAC) due to a gradient in water potential is illustrated in Figure 2.1. An upward flow of water occurs when water potential within the SPAC is lowest in the atmosphere and highest in the soil. Water potential in the atmosphere is generally low when atmospheric relative humidity is low or when temperature is high, leading to a high vapour pressure deficit (VPD). VPD is the difference between the saturation vapour pressure at leaf temperature and the actual vapour pressure of the air. Since the air spaces within leaves are typically saturated, VPD effectively drives transpiration. The steep potential gradient at the leaf surface leads to water loss from the leaves to the atmosphere. Due to the strong cohesive forces between neighbouring water molecules, negative hydrostatic pressure [20] occurs in the xylem, forcing water to be pulled upward. The cohesive properties of water maintain a continuous column from the roots to the leaves, enabling the continuous movement of water from the soil, through the stem, and into the atmosphere.

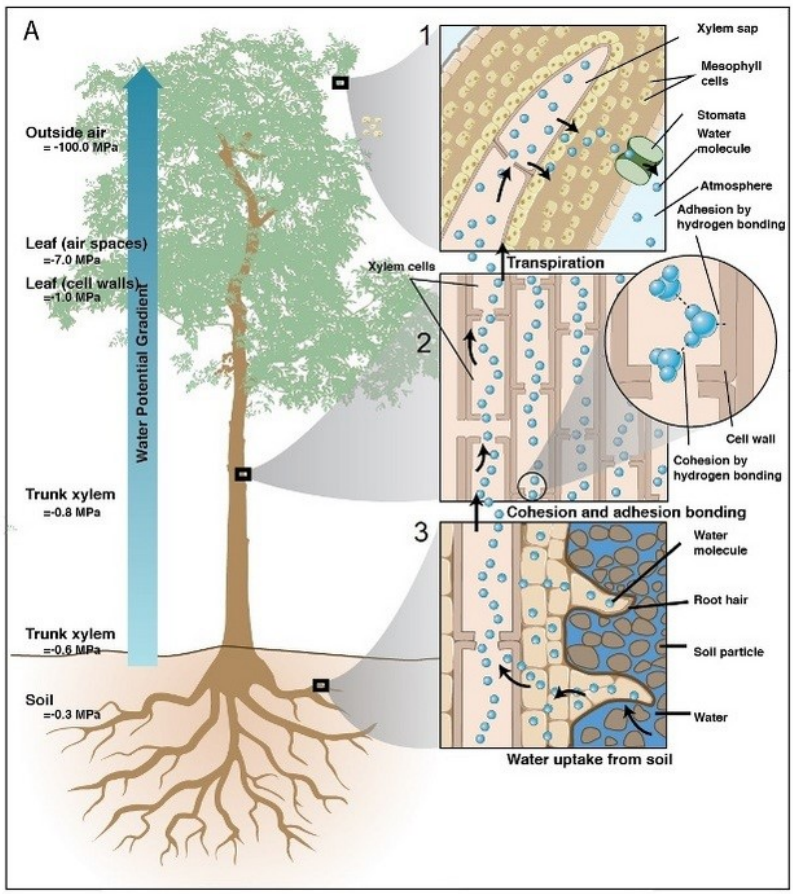

Figure 2.1: Illustration of water movement within the soil-plant-atmosphere continuum. Water moves from high water potential in the soil through the tree to low water potential in the atmosphere. ©2013 Nature Education. Reprinted with permission from [19].

Water stored in stems, branches, and foliage can act as a buffer when transpirational demands are high [21]. Horizontal redistribution of water within the stem [17] occurs when there is a difference in water potential between the xylem and surrounding tissues, leading to withdrawal of water from the storage tissue and to effective shrinkage of the stem [22]. As a result of this dynamic storage, variations in total tree water content occur.

2.2 Measurement of Tree Water Variables

There exist a number of variables that are used to quantify tree water dynamics. In the following, the focus will lie on measurements and planned measurements

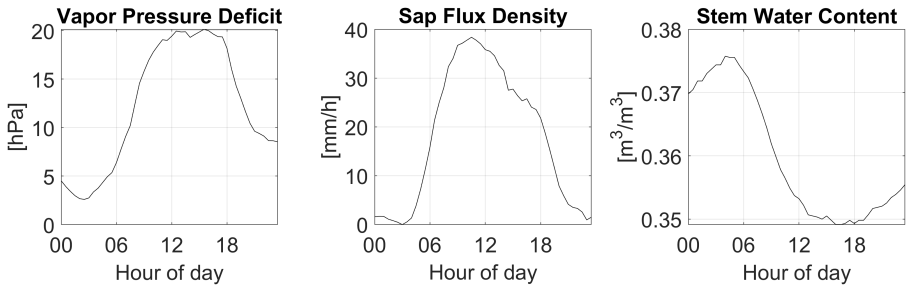

Figure 2.2: Diurnal variations in vapour pressure deficit (VPD), sap flow and stem water content during May 18, 2024, in the Svartberget Experimental Forest in northern Sweden. VPD is estimated from temperature and relative humidity measurements [32]. Sap flux density and stem water content are from point measurements in a single pine tree [33].

within the forest area of interest to this thesis that is located within the Svartberget Experimental Forest in northern Sweden [23].

Instruments used to quantify tree water dynamics at the tree level collect generally invasive point measurements. Dendrometers [24] measure changes in stem radius at a specific point on the tree trunk or branch which can be used to quantify changes in stored water content in the elastic phloem tissue of the tree. Sap flow sensors measure water flow within the hydrologically active xylem of the tree using typically heat-based methods [25], where a heat pulse is emitted, and the temperature difference between two probes is measured to determine the sap flow rate. Tensiometers measure water potential [26] in soils [27] or tree stems [28]. Soil moisture sensors have been successfully used to measure volumetric water content in tree stems [29]. Capacitance-type soil sensors measure the charging time that depends on the dielectric permittivity of the material in which the probe is inserted. In soils, as well as in trees, the dielectric permittivity is dominated by the volume fraction of liquid water [30]. In soils, a calibration curve is used to convert the measured charging time to soil moisture content. If inserted in a tree stem, the sensors have to be recalibrated to the wood density of the specific tree species to measure volumetric water content. All these in situ sensor require relatively high maintenance and rely on data loggers and power supplies for functioning.

Water transport in trees is closely linked to atmospheric conditions, which influence transpiration demand. Atmospheric parameters at the stand- to ecosystem scale are in general measured non-invasively. ET can be estimated from latent heat flux measurements using flux towers [31]. VPD can be calculated from measurements of air temperature and relative humidity.

Figure 2.2 illustrates the temporal connection between different tree water dynamics variables in the course of a rain-free summer day in the Svartberget Experimental Forest. When temperature rises in the morning and relative humidity in the air decreases, VPD rises. Photosynthesis starts which leads to decreased internal CO_2 concentrations, which causes the stomata to open. This leads to the onset of transpiration leading to the start of sap flow within

the stem. VPD continues to increase until reaching a peak at midday, which leads to an increase in sap flow with a peak around midday. The increasing high water demand in the morning leads to a decrease in stem water content when water reservoirs are depleted. When VPD and sap flow decrease in the afternoon and sap flow drops to zero during the night, stem water reserves are refilled again as it can be seen from the increase in stem water content.

While the different measurement techniques offer valuable insights into the water transport within trees and its relationship to atmospheric drivers, measuring the full SPAC remains a challenge. Temperature, humidity, and water availability vary across locations, making it difficult to derive a single representative VPD or ET value for a forest stand [34]. VWC and sap flow vary with height, radial position, and exposure (e.g., north vs. south-facing sides), complicating upscaling to whole-tree water budgets. Wind conditions influence the area measured by ET sensors, causing temporal variations in their representativeness. Separating soil evaporation from plant transpiration remains an ongoing research challenge [35].

To overcome the limitations of current in situ sensors, models can be used to link tree water variables and describe the SPAC over larger spatial scales.

2.3 Modelling Tree Water Dynamics

SPAC models work by simulating the interactions and processes that govern the movement of water from the soil, through plants, and into the atmosphere.

Most of the practical models are defined on a landscape scale. Upscaling from leaf and plant scales to landscape scales is one of the challenges that SPAC models face [36]. As mentioned in Section 2.2, measurements quantifying forest water dynamics are made at different scales. Point measurements of tree water dynamics, such as sap flow and tree radius changes, must be upscaled to the tree level and then related to meteorological or flux measurements, e.g., VPD and ET, at a stand or landscape scale.

Simple models at the tree scale have been developed [37] and expanded [38]. A version of the model described in [38], assuming constant soil water potential, was calibrated using sap flow measurements and dendrometer data of several trees in the study area (see Figure 2.3) that was used in this thesis. The model input was a transpiration time series estimated from the ET measured by a flux tower which had a flux footprint overlapping with the study area. Figure 2.4 shows transpiration estimated from ET used as a model input and internal tree water fluxes and water potentials estimated by the model output over 15 days in summer 2023. The cyclic nature of tree water variables is due to the depletion and refilling of internal water reserves.

Most hydraulic models require complicated calibration and were developed for trees under controlled conditions [37], [39]. Outputs under natural conditions do not agree well with in-situ VWC measurements, especially for long-term trends, if no further calibration is applied. Therefore, in this thesis, the focus is placed on linking in situ sensor measurements directly to radar measurements.

Figure 2.3: Photograph of the forest under study in this thesis. A point dendrometer is installed on the tree at the centre of the image.

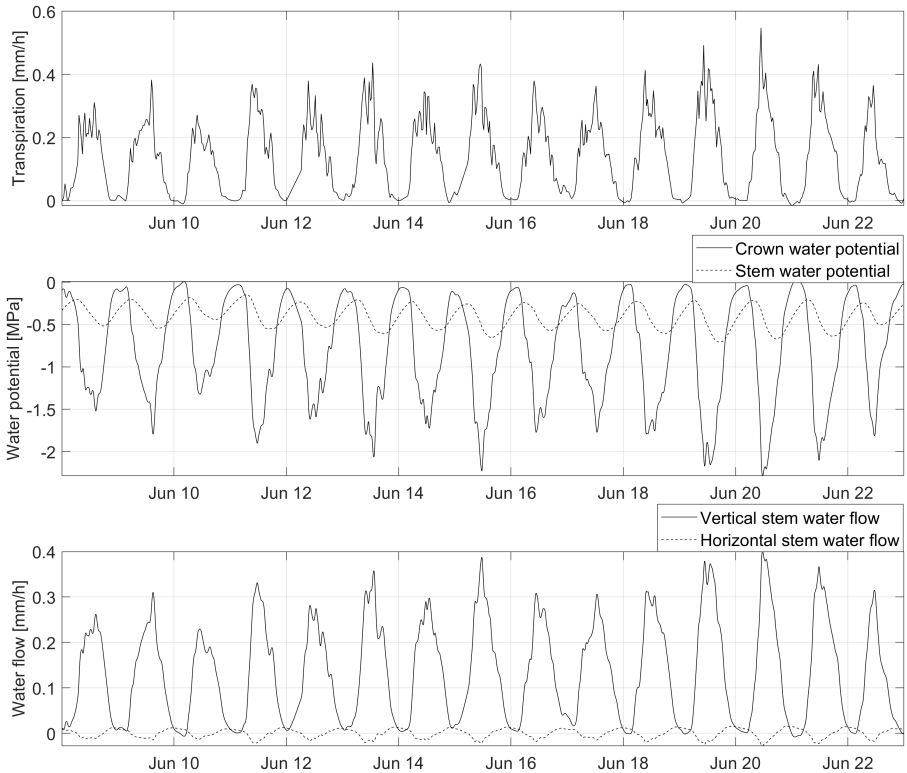

Figure 2.4: Input and output of a hydraulic tree dynamics model based on [38]. Transpiration in the top graph is derived from ET measured by the ICOS flux tower [32] and scaled to match a single tree transpiration. The model was calibrated using sap flow and dendrometer measurements during a 15-day period in summer 2024. Model outputs are crown and stem water potential given in the middle graph. Vertical stem water flow as well as horizontal stem water flow, i.e. water flow from phloem to xylem are shown in the bottom graph.

Chapter 3

Radar Remote Sensing of Forests

Remote sensing of Earth surface variables is widely used, and with an increasing number of new satellites launched [40]–[45], more options are available for global-scale monitoring of Earth observables [46]. Passive sensors receive signals from the Earth and rely on reflected sunlight and thermal radiation emitted by the Earth. Active sensors transmit signals that are scattered and received by the sensor. In particular SAR, which is an active sensor, is promising for mapping forest water variables remotely due to a number of properties and advantages in comparison to other Earth observation techniques:

1. SAR systems operate from moving platforms, e.g. satellites or airplanes. By combining signals from multiple radar pulses over time, they achieve fine spatial resolution (1 to 50 m) while offering wide area coverage (10 to 500 km swath). This gives SAR systems a distinct advantage over other microwave remote sensing sensors, whose resolution is limited by the physical antenna size.

2. Radar systems operate in the microwave region of the electromagnetic spectrum, which allows them to penetrate through clouds, rain, and smoke, in contrast to optical sensors. Because they are active sensors, radar systems can operate independent of the availability of e.g. sunlight as needed for optical sensors. This makes radar remote sensing independent of weather conditions and usable both day and night, providing consistent observations.

3. Microwaves interact with forest components such as trunks, branches, leaves, and soils. The radar backscatter intensity depends on the dielectric and geometric properties of the forest, which are dominated by the liquid water content and its spatial distribution. This makes radar particularly sensitive to changes in VWC, making it promising for monitoring forest water status and dynamics.

4. Depending on the frequency band used, radar can penetrate the forest canopy to varying depths, making them sensitive to different forest structures. Lower frequency bands, such as P-band (420–450 MHz), penetrate deeper into the forest as they are less attenuated and become sensitive to larger tree structures such as branches and stems. In contrast, higher frequencies, such as C-band (4–8 GHz), are scattered and attenuated by smaller structures such as branches and leaves, making them more sensitive to the upper forest canopy.

5. Some SAR systems use multiple flight paths, providing observations of a scene from multiple incidence angles. This provides vertical resolution, a technique called radar tomography. Radar tomography separates backscatter contributions from different heights, which is particularly useful for understanding the vertical distribution of water across different forest layers, separating VWC dynamics from soil water dynamics.

3.1 Speckle

In radar remote sensing of distributed scatterers, an important phenomenon to account for is speckle. A forest can be treated as a randomly distributed ensemble of scattering elements (e.g. leaves, branches, stems and ground). The average scattering intensity (radar cross section) per area of such a distributed target can be described in terms of the backscattering coefficient σ^0. The backscattering coefficient at a given frequency, polarisation and incidence angle is, through electromagnetic interactions, related to the dielectric and geometric properties of the forest.

However, the radar signal received from a single resolution cell is the coherent sum of the complex amplitudes of all individual scatterers within that cell. Due to the coherent sum, a single radar measurement does, in general, not provide a good estimate of the backscattering coefficient. Instead, it exhibits random fluctuations due to constructive and destructive interference between scattered waves, leading to multiplicative noise in images known as speckle.

The influence of speckle variations on the backscatter estimate can be reduced by taking an ensemble average over several independent measurements of the same distributed target. Averaging can be performed in space over a homogeneous area or by dividing the frequency content into sub-bands. If dielectric properties of the forest remain constant between two measurement acquisitions, and the measurements are decorrelated, averaging can even be applied over time to reduce speckle.

The effect of averaging on the probability distribution of the backscatter estimate is illustrated in Figure 3.1. When no averaging is applied, the backscatter intensity follows a negative exponential distribution, where the mean and standard deviation (SD) are equal to the true backscattering coefficient, i.e., $\frac{\mathrm{SD}}{\sigma^0} = 1$. With a higher number of independent samples that are averaged, the probability density function becomes narrower. While the mean still equals the backscattering coefficient, the standard deviation is reduced by a factor $1/\sqrt{N}$, where N is the number of independent measurements, resulting in $\frac{\mathrm{SD}}{\sigma^0} = \frac{1}{\sqrt{N}}$.

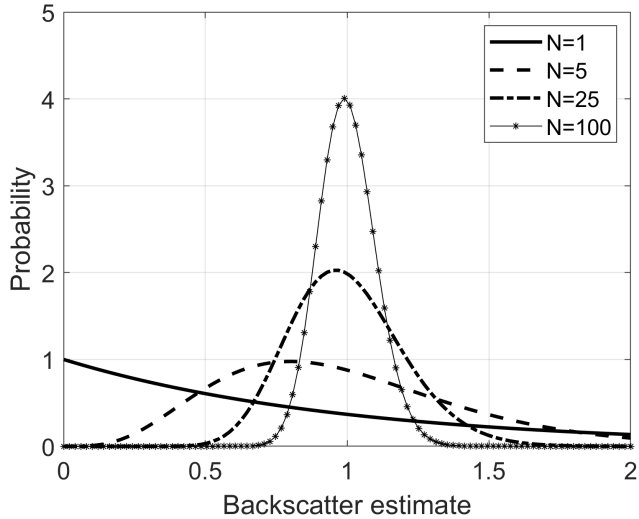

Figure 3.1: Probability distribution of the backscatter estimate from averaging N independent samples [47]. The backscatter mean is 1 for all distributions.

Radiometric resolution can be defined as the ratio between standard deviation and mean of backscatter, i.e. it is a measure of the spread of backscatter due to speckle variations. Achieving fine radiometric resolution requires averaging many independent samples N, which improves radiometric resolution by a factor of $1/\sqrt{N}$. For a distributed target like a forest, this can be accomplished through spatial averaging. Therefore, there is a trade-off between radiometric resolution and spatial resolution.

In Paper II, a different definition of radiometric resolution is used, as the time series are presented in dB scale. Here, radiometric resolution is defined as the standard deviation of logarithmic backscatter.

3.2 Spaceborne Synthetic Aperture Radar

The number of spaceborne SAR systems are steadily increasing [40]–[46], [48]–[53]. Electromagnetic waves at different frequencies exhibit different scattering behaviours, making them sensitive to various structures and water pools within the forest. The operating frequency bands of current and upcoming SAR satellites lie within the range from P-band (420–450 MHz) to X-band (8–12 GHz), all of which are of interest for monitoring different forest variables.

Currently, the spaceborne SAR with the lowest frequency operates within the L-band (1–2 GHz). ALOS-2 PALSAR-2 and ALOS-4 PALSAR-3 by JAXA acquire images at different observation modes at resolutions from 1×3 m to 100 m [48], [49]. The number of observations at a certain observation mode per year and region varies depending on JAXA's observation schedule and user specific observation requests according to the Basic Observation Scenario (BOS). The two SAOCOM satellites by CONAE, also operating at L-band,

have different observation modes with resolutions between 10 and 100 m [50]. Mostly, the low-resolution operation mode is used for increased spatial coverage. Spaceborne SAR tomography was recently demonstrated for the first time using SAOCOM observations [54]. Two upcoming L-band satellite missions are close to launch. NISAR, a joint mission by NASA and ISRO, is planned for launch in 2025. NISAR will also feature an S-band (2–4 GHz) SAR. NISAR's highest resolution mode (3 to 10 m) will continuously acquire data. NISAR will have a revisit time of 12 days for global coverage [41]. ROSE-L by ESA is planned for launch 2028. ROSE-L is planned to have a revisit time of 3 to 6 days depending on the observation mode [43].

C-band (4 – 8 GHz) is widely used for land applications using the Sentinel-1 satellites by ESA [51], [55]. The current constellation includes Sentinel-1A, launched in 2014, and Sentinel-1C, launched in 2024. Sentinel-1B, launched in 2016, failed and was retired in 2021. The satellites (Sentinel-1A and 1C) are orbiting 180° out of phase, offering a 6-day repeat cycle by combining the individual 12-day repeat cycles. The most commonly used observation mode of Sentinel-1 provides a resolution of 5 x 20 m [45]. Other SAR satellite missions at C-band include RADARSAT-2 and the RADARSAT constellation mission (RCM) by CSA. RADARSAT-2 is a single satellite [52] whereas RCM consists of three identical satellites [56]. These satellites achieve, depending on operation mode, resolutions, between 1 m and 100 m. RADARSAT-2 has a 24-day revisit cycle. RCM has a shorter revisit time, with some points of the Earth imaged up to four times a day.

Several SAR satellite constellations are currently operating at X-band. TanDEM-X by DLR consists of two X-band SAR satellites orbiting in close formation [53]. ICEYE currently operates 27 microsatellites with X-band SAR systems [57], providing fine resolution and short revisits. Capella Space operates a constellation of currently 19 X-band SAR satellites, providing high-resolution imagery [58]. Umbra Space operates a constellation of microsatellites with X-band SAR systems, providing high-resolution imagery. The Umbra constellation is planned to contain 32 satellites [59].

No spaceborne SAR system is currently operating at P-band. The BIOMASS satellite by ESA, planned for launch in 2025, will be the first spaceborne P-band SAR. The satellite will feature a tomographic and interferometric SAR with a near 3-day repeat cycle. The mission will last for five years and will comprise a 14-month tomographic phase followed by an interferometric phase. BIOMASS will not acquire data over Europe and North America due to ITU Radio Regulations [13], [40].

Spaceborne SAR systems have in general a large, often global, coverage. Spatial resolutions can go down to the order of meters, however, temporal resolution is in general coarse and of the order of days to weeks. Current SAR missions do not feature tomographic modes, so no vertical resolution is acquired. To study forest processes on shorter time scales or smaller spatial scales, and to separate processes in different forest layers, radar systems with very high temporal and spatial resolution are needed. Tower-based radar systems can provide both and improve our understanding of forest backscatter observed by satellites.

(a) BorealScat radar tower.

(b) BorealScat-2 radar tower.

Figure 3.2: The two BorealScat radar towers. BorealScat was operating in Remningstorp in southern Sweden until 2021. In 2022, BorealScat was moved to the Svartberget Experimental Forest located in northern Sweden and upgraded to BorealScat-2 to include a horizontally moving antenna frame.

3.3 Tower-Based Radar

There are only a handful of radar tower experiments conducted in forests. The TropiScat [60] and AfriScat [61] radar towers, located in French Guiana and Ghana, respectively, have acquired multi-polarimetric tomographic radar observations of tropical forests at P- and L-band. In 2018, TropiScat was upgraded to TropiScat-2 [62], which also included C-band non-tomographic observations. SAR observables, mostly coherence, were studied over time scales ranging from hours to months [60]–[62].

Three radar towers have been used to observe boreal forests. The SodSAR experiment, a multi-polarimetric SAR located in Finland, has been utilized to study SAR observables of a sparse boreal forest at L-, C-, and X-band [63]. The radar system is mounted on a rail, allowing it to operate in a SAR mode.

The BorealScat experiment, shown in Figure 3.2(a) operated between 2017 and 2021 in southern Sweden, acquiring multi-polarimetric observations of a hemi-boreal forest at P-, L-, and C-band [14]. Tomographic images were produced at all frequency bands. Due to short measurement durations, this radar tower acquired the first tomographic images that were robust to wind-induced tree movement. The radar measurements had a very high temporal resolution, with measurements taken every 5 minutes. These measurements

consisted of the average of four repeated measurement in order to improve radiometric resolution [14]. In low wind conditions, these four measurements were highly correlated, thus no significant improvement of radiometric resolution was achieved. In windy conditions, the measurements were partly decorrelated and could be averaged to improve radiometric resolution [14].

In 2022, the tower was moved to northern Sweden to observe a boreal forest and was reconstructed as BorealScat-2, shown in Figure 3.2(b). Tomographic images were again produced at all frequency bands. The new set-up incorporated a horizontally moving antenna frame at L- and P-band, i.e., effectively a tomographic SAR system, and a fixed radar at C-band [16], [64]. The moving antenna frame is however not mainly used to reconstruct 3D tomograms, as the image focus depends on scene decorrelation. Instead, the images acquired during the measurement sequence are treated as independent samples and averaged to a new 2D image with improved radiometric resolution [16]. One measurement of this kind is acquired every 30 minutes.

The number of independent samples N_a along the track which the antenna array moves on can be calculated as

$$N_a = \frac{4L}{\lambda} \sin \frac{\beta_h}{2}, \tag{3.1}$$

where β_h is the horizontal antenna beam width and L is the length of the track. Equation (3.1) follows from Equation (14.123) in [65] when inserting Equation (14.34) in [65] and observation time ($T = L/u$), where u is the velocity of the frame. For BorealScat-2 $\beta_h \approx 90^{\text{o}}$ and $L = 4$ m. For P- and L-band, N_a is, hence, 16 and 49, respectively. This means, the number of independent samples is improved by these factors due to the moving antenna frame.

As discussed in Section 3.1 this higher number of independent samples gives a finer radiometric resolution compared to BorealScat, resulting in backscatter estimates of higher precision [16]. This allows to study small backscatter variations without additional averaging in time or space, resulting in tomograms with finer temporal, spatial and radiometric resolution than any other radar tower has ever provided.

The studies described in the papers appended to this thesis were conducted using observations from both BorealScat and BorealScat-2.

3.4 Modelling Radar Backscatter of Forest

SAR observables obtained over forests can be linked to the forest variables introduced in Section 2. In this section, the dependency of the backscattering coefficient on several forest variables will be briefly discussed.

The scattering of an electromagnetic wave at a given frequency and polarisation from a non-magnetic object can theoretically be calculated if the dielectric properties, shape, and orientation of the object are known. In forests, the dielectric constant is predominantly influenced by water content in vegetation and soil, directly linking backscatter to water-related forest variables. However, even with a detailed description of all forest components, including their

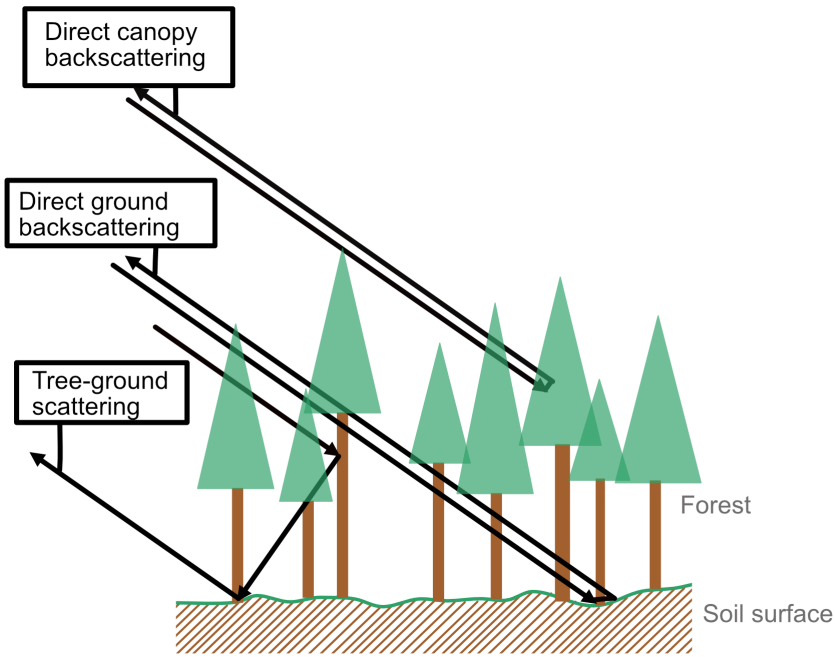

Figure 3.3: Illustration of the dominant scattering mechanisms in a forest.

geometry and dielectric constant, solving the scattering problem analytically is infeasible. Numerical methods can be applied to a discretized forest, but the computational cost remains extremely high.

Approximative forest scattering models, while less accurate, are more practically invertible for the retrieval of forest parameters due to the fewer number of model parameters. These models are particularly valuable for applications such as spaceborne SAR missions, where in situ data are limited.

Most forest backscatter models represent forests as consisting of three primary components: tree trunks, tree canopy, and the ground surface. According to radiative transfer theory, when only single scattering effects within the canopy are considered, the different backscattering contributions can be attributed to three main scattering mechanisms as illustrated in Figure 3.3. Under the assumption that the extinction coefficient κ_e that accounts for absorption and scattering losses is uniform within the full canopy, attenuation of p-polarised waves through the canopy can be modelled as

$$L_p = \exp\left(\frac{\kappa_{e_p} d}{\cos\theta_i}\right), \tag{3.2}$$

where d is the canopy height and θ_i is the incidence angle of the radar wave. Denoting receive/transmit polarisations pq, the backscattering contributions illustrated in Figure 3.3 can be described as follows [65]:

1. Direct ground backscatter occurs when the incident wave is scattered back towards the radar by the ground. It can be expressed as

$$\sigma^0_{g_{pq}} = \sigma^0_{s_{pq}} L_p^{-1} L_q^{-1}, \tag{3.3}$$

where σ^0_s is the backscattering coefficient of the ground surface.

2. Direct canopy backscatter occurs directly from all canopy elements (stems are also included here) at various heights within the canopy. Assuming that the canopy can be represented as a homogeneous layer, the canopy backscatter can be modelled as

$$\sigma^0_{c_{pq}} = \frac{\sigma^{back}_{v_{pq}} \cos\theta_i}{\kappa_{e_p} + \kappa_{e_q}} \left(1 - L_p^{-1} L_q^{-1}\right), \tag{3.4}$$

where σ^{back}_v is the volume backscattering coefficient of the vegetation medium.

3. Double-bounce scattering between ground surface and canopy or trunk describes a process where the electromagnetic wave is first scattered from vegetation element towards the ground and then reflected back towards the radar. This process can also occur in reverse order. The strength of this scattering contribution is particularly significant at lower frequency bands (P- to L-band) due to reduced attenuation and the effect of ground roughness and stronger interactions with tree trunks. Assuming a relatively flat surface in comparison to the wavelength, coherent addition of the vegetation-ground and ground-vegetation scattering can be applied and the double-bounce scattering can be modelled as

$$\sigma^0_{cg_{pp}} = 4\sigma^{bist}_{v_{pp}} d\Gamma_p L_p^{-2}, \tag{3.5}$$

where σ^{bist}_v is the bistatic volume scattering coefficient and Γ is the Fresnel reflectivity.

All mentioned backscattering contributions are directly linked to the dielectric properties of the canopy through attenuation which depends on the dielectric properties of the canopy and for direct canopy and tree-ground scattering through the backscatter or bistatic scattering, respectively. In the simplest canopy backscattering model, the water cloud model, vegetation is modelled as a homogeneous volume of identical scatters, an equivalent water cloud [66]. Then the water content of this water cloud, representing the VWC, can be directly related to backscatter observed by a radar. However, the water cloud model fails to explain the observed backscatter time series at L-band by BorealScat-2, an issue addressed in Paper II.

The direct ground backscatter and the Fresnel reflectivity in the tree-ground scattering depend in addition on the dielectric properties of the ground surface. Hence, soil moisture of the ground and water content at all vegetation heights directly relates to the forest backscatter through their influences on the dielectric

constant. Thus, changes in these forest water variables will lead to changes in backscatter.

The relationship of water within the forest to forest backscatter is exploited when trying to estimate soil moisture content [67], [68] and above-ground biomass [69] from SAR systems observing forests. Estimation of forest VWC from SAR backscatter has not been evaluated yet and is addressed in Paper II.

Chapter 4

Summary of Appended Papers

4.1 Paper I: Comparison of Tower-Based and Satellite L- and C-Band Radar Backscatter from a Boreal Forest

One objective of observing forests with tower-based radar is to enhance the understanding of forest scattering mechanisms to improve forest variable retrieval algorithms for spaceborne SAR missions. However, the relevance of tower-based observations for satellite observations has not been verified yet.

This paper evaluates the applicability of tower-based radar observations for spaceborne SAR missions by comparing Sentinel-1 and ALOS-2 PALSAR-2 products with BorealScat radar tower backscatter at L- and C-band.

At C-band, the tomographic capabilities of the BorealScat tower were used to integrate intensity over a canopy-region of interest and a full forest region of interest, producing both canopy-only and full forest backscatter time series. At L-band, full forest backscatter time series were produced from BorealScat tomograms. Sentinel-1 products were used to produce backscatter time series of the BorealScat footprint and a larger region of interest in a reference forest close to the BorealScat tower. ALOS-2 PALSAR-2 products were used to produce backscatter time series of a BorealScat forest stand region of interest. A 14-month backscatter time series for L-band and a 3.5-year backscatter time series for C-band were produced. The C-band time series included tree deaths in the BorealScat forest stand due to a bark beetle infestation in the end of the time series.

For the healthy forest, the agreement between BorealScat and Sentinel-1 observations was within 0.9 dB (RMSE) for C-band. However, a significant drop in canopy-only backscatter was observed during the time period of forest dieback. The drop was less significant in the full forest backscatter observed by BorealScat and not observed in the Sentinel-1 observations. It is hypothesized

that in the case of tree deaths the contribution of the ground backscatter increased due to decreased canopy attenuation. At L-band, the agreement of BorealScat and ALOS-2 PALSAR-2 observations was within 0.6 dB (RMSE).

This first-ever comparison of tower-based and spaceborne radar time series demonstrated that BorealScat indeed provided relevant observations for spaceborne SAR missions. However, the lack of vertical resolution of current C-band SARs severely limits their ability to provide useful information about forest canopies. With upcoming tomographic SAR missions, spaceborne radar holds the potential to observe forest dynamics with a quality matching needs of applications.

Contribution to the paper: I processed the spaceborne SAR data and produced the data analysis results. Interpretation of the results was done together with my co-authors. I prepared the manuscript together with A. R. Monteith, with finalization involving all co-authors.

4.2 Paper II: Estimation of Stem Water Content from Tower-Based L–Band Radar Backscatter of a Boreal Forest

Radar is highly sensitive to VWC. While models linking radar backscatter to biomass [68], [70]–[72] or directly to VWC [73] have been proposed, no in situ forest VWC measurements have yet been used to train or validate those models. This paper investigates the relationship between VWC and tower-based L-band radar backscatter in a boreal forest. It also explores the potential of using the proposed backscatter model for VWC retrieval.

Earlier observations have shown that BorealScat-2 radar tower backscatter at L-band peaks during mid day and has minima during the night [16], an anomaly that cannot be explained by the original water cloud model [66]. In this study, an extended water cloud model that treats the relationships of attenuation and scattering on VWC separately was employed to link forest backscatter and stem water content. Tomographic images at L-band produced by BorealScat-2 during rain-free time periods, spanning approximately one month in total, were used to extract time series of canopy backscatter and relative attenuation. These time series, combined with in situ stem water content measurements, allowed for the estimation of the model parameters.

The parameter estimation process confirmed that only model coefficients that correspond to a ratio of volume backscattering coefficient and extinction that anticorrelates with VWC are able to describe the observed canopy backscatter-VWC relationship. The stem water content estimated from canopy backscatter aligned well with the diurnal and long-term trends observed in the measured stem water content. However, during a short time period a small drop in average backscatter occurred, while average attenuation remained unchanged. During these days, which coincided with low VPD variability, the

backscatter model overestimated stem water content. The attenuation-based model outperformed the canopy backscatter model, particularly during these days. In both models, a phase shift occurred between the modelled and measured stem water content, suggesting that the modelled stem water content represents a different tree water pool, likely located higher up in the canopy, compared to the in situ stem water measurements.

This is the first time that forest stem water content was extracted from tower-based radar observations and compared to high-quality in situ stem water observations. The results demonstrate that variations in canopy backscatter observed at L-band by the BorealScat-2 experiment can be effectively captured by the proposed model, making the inversion of canopy backscatter to VWC feasible. These findings further emphasize the potential of tomographic L-band spaceborne SAR missions for monitoring forest VWC.

Contribution to the paper: I designed the model with L. M. H. Ulander. I processed the data from tomographic images, performed the model parameter estimation process, produced the data analysis results and prepared the manuscript. Interpretation of the results and finalization of the manuscript was done together with the co-authors.

Chapter 5

Future Work

The aim of this thesis was to establish a link between spaceborne SAR observables and VWC in a boreal forest. In the first paper, the relevance of tower-based radar observations for spaceborne SAR observations was investigated at C- and L-band comparing BorealScat data to Sentinel-1 and ALOS-2 PALSAR-2 data. Currently, additional in situ measurements are taken and planned to be taken near the BorealScat-2 radar tower. Therefore, the relevance of tower-based radar observations for spaceborne SAR data at this site is planned to be further investigated. This will involve comparing C- and L-band BorealScat-2 tower observations with spaceborne SAR data from new satellite missions such as NISAR (planned to be launched in 2025), ALOS-4 (launched in 2024), as well as additional C-band data from the dual-satellite Sentinel-1 mission operating again.

In the second paper, a model that links canopy backscatter and forest VWC was tested for BorealScat-2 L-band backscatter with promising results. However, further refinement and calibration of the backscatter model is necessary. In 2025, additional in situ sensors will be installed in trees within the footprint of the BorealScat-2 tower. This includes more stem water sensors, also located higher up in the trees, and water potential sensors in several trees. These installations aim to provide new data for VWC inversion models by the end of 2025. This will allow the incorporation of more training and validation data to further develop the backscatter model.

So far, the modelling work was focused on L-band, but also other frequency bands are of interest and could be tested for the used model. Data is currently acquired at C-, UHF-, and P-bands, for which a validity of the model could be tested. Additionally, an X-band radar is scheduled for installation in spring 2025. Data acquisition is still ongoing and possibly new forest events, e.g., droughts, will be captured and analysed.

Although the upcoming BIOMASS mission will not acquire data over Europe, forest sites within its observation area with already existing in situ data have been identified and could be studied in the future to examine the effect of variation in forest VWC on spaceborne SAR backscatter at P-band.

The conducted and planned research will further advance the development

of a retrieval algorithm for VWC based on spaceborne SAR data.

Bibliography

[1] P. Artaxo, H.-C. Hansson, M. Andreae *et al.*, "Tropical and boreal forest – atmosphere interactions: A review," *Tellus B*, vol. 74, pp. 24–163, 2022. DOI: 10.16993/tellusb.34 (cit. on p. 3).

[2] Y. Pan, R. Birdsey, O. Phillips *et al.*, "The enduring world forest carbon sink," *Nature*, vol. 631, pp. 563–569, 2024. DOI: 10.1038/s41586-024-07602-x (cit. on p. 3).

[3] A. M. Wani and G. Sahoo, "Forest ecosystem services and biodiversity," in *Spatial Modeling in Forest Resources Management : Rural Livelihood and Sustainable Development*, P. K. Shit, H. R. Pourghasemi, P. Das and G. S. Bhunia, Eds. Springer International Publishing, 2021, pp. 529–552. DOI: 10.1007/978-3-030-56542-8_22 (cit. on p. 3).

[4] G. Bonan, "Forests and climate change: Forcings, feedbacks, and the climate benefits of forests," *Science (New York, N.Y.)*, vol. 320, pp. 1444–9, 2008. DOI: 10.1126/science.1155121 (cit. on p. 3).

[5] R. Keenan, "Climate change impacts and adaptation in forest management: A review," *Annals of Forest Science*, vol. 72, 2015. DOI: 10.1007/s13595-014-0446-5 (cit. on p. 3).

[6] K. Steppe, "The potential of the tree water potential," *Tree Physiology*, vol. 38, no. 7, pp. 937–940, 2018. DOI: 10.1093/treephys/tpy064 (cit. on p. 3).

[7] N. Grulke, C. Bienz, K. Hrinkevich, J. Maxfield and K. Uyeda, "Quantitative and qualitative approaches to assess tree vigor and stand health in dry pine forests," *Forest Ecology and Management*, vol. 465, p. 118 085, 2020. DOI: 10.1016/j.foreco.2020.118085 (cit. on p. 3).

[8] R. Massey, L. T. Berner, A. C. Foster, S. J. Goetz and U. Vepakomma, "Remote sensing tools for monitoring forests and tracking their dynamics," in *Boreal Forests in the Face of Climate Change: Sustainable Management*, M. M. Girona, H. Morin, S. Gauthier and Y. Bergeron, Eds. Springer International Publishing, 2023, pp. 637–655. DOI: 10.1007/978-3-031-15988-6_26 (cit. on p. 3).

[9] K. Rao, W. R. Anderegg, A. Sala, J. Martínez-Vilalta and A. G. Konings, "Satellite-based vegetation optical depth as an indicator of drought-driven tree mortality," *Remote Sensing of Environment*, vol. 227, pp. 125–136, 2019, ISSN: 0034-4257. DOI: https://doi.org/10.1016/j.rse.2019.03.026. [Online]. Available: https://www.sciencedirect.com/science/article/pii/S0034425719301208 (cit. on p. 3).

[10] A. Konings, S. Saatchi, C. Frankenberg *et al.*, "Detecting forest response to droughts with global observations of vegetation water content," *Global Change Biology*, vol. 27, 2021. DOI: 10.1111/gcb.15872 (cit. on p. 3).

[11] Q. Chen, R. Mcroberts, C. Wang and P. Radtke, "Forest aboveground biomass mapping and estimation across multiple spatial scales using model-based inference," *Remote Sensing of Environment*, vol. 184, pp. 350–360, 2016. DOI: 10.1016/j.rse.2016.07.023 (cit. on p. 3).

[12] S. Hancock, C. Mcgrath, C. Lowe, I. Davenport and I. Woodhouse, "Requirements for a global lidar system: Spaceborne lidar with wall-to-wall coverage," *Royal Society Open Science*, vol. 8, 2021. DOI: 10.1098/rsos.211166 (cit. on p. 3).

[13] S. Quegan, T. Le Toan, J. Chave *et al.*, "The European Space Agency BIOMASS mission: Measuring forest above-ground biomass from space," *Remote Sensing of Environment*, vol. 227, pp. 44–60, Jun. 2019. DOI: 10.1016/j.rse.2019.03.032 (cit. on pp. 4, 14).

[14] L. M. H. Ulander, A. R. Monteith and M. Rönnfalk, "Borealscat final report," European Space Agency (ESA), Tech. Rep. Contract 4000118576/16/NL/FF/mg, 2019. [Online]. Available: https://earth.esa.int/eogateway/campaigns/borealscat (cit. on pp. 4, 15, 16).

[15] L. M. H. Ulander and A. R. Monteith, "Borealscat contract change notice 1 final report," European Space Agency (ESA), Tech. Rep. Contract 4000118576/16/NL/FF/mg, 2022. [Online]. Available: https://earth.esa.int/eogateway/campaigns/borealscat (cit. on p. 4).

[16] A. R. Monteith, L. M. H. Ulander, S. C. Steele-Dunne *et al.*, "A tower-based radar experiment for studying the effects of boreal forest tree-water relations," *SSRN Electronic Journal. Preprint*, 2024, Available at SSRN: http://dx.doi.org/10.2139/ssrn.4991471. DOI: 10.2139/ssrn.4991471 (cit. on pp. 4, 16, 22).

[17] S. Pfautsch, J. Renard, M. Tjoelker and A. Salih, "Phloem as capacitor: Radial transfer of water into xylem of tree stems occurs via symplastic transport in ray parenchyma," *Plant physiology*, vol. 167, 2015. DOI: 10.1104/pp.114.254581 (cit. on pp. 5, 6).

[18] H. Lambers and R. S. Oliveira, "Plant water relations," in *Plant Physiological Ecology*, Springer Nature Switzerland AG, 2019, pp. 302–416 (cit. on p. 5).

[19] A. McElrone, B. Choat, G. Gambetta and C. Brodersen, "Water uptake and transport in vascular plants," *Natue Education Knowledge*, vol. 4, 2013 (cit. on p. 6).

[20] P. F. Scholander, H. T. Hammel, E. D. Bradstreet and E. A. Hemmingsen, "Sap pressure in vascular plants," *Science*, vol. 148, no. 3668, pp. 339–346, 1965. [Online]. Available: http://www.jstor.org/stable/1715071 (visited on 17/12/2024) (cit. on p. 5).

[21] J. Landsberg, R. Waring and M. Ryan, "Water relations in tree physiology: Where to from here?" *Tree Physiology*, vol. 37, no. 1, pp. 18–32, 2017. DOI: 10.1093/treephys/tpw102 (cit. on p. 6).

[22] K. M. Herzog, R. Häsler and R. Thum, "Diurnal changes in the radius of a subalpine norway spruce stem: Their relation to the sap flow and their use to estimate transpiration," *Trees*, vol. 10, pp. 94–101, 1995. [Online]. Available: https://api.semanticscholar.org/CorpusID:36486077 (cit. on p. 6).

[23] H. Laudon, E. Hasselquist, M. Peichl *et al.*, *Northern landscapes in transition; evidence, approach and ways forward using the krycklan catchment study*, 2020. DOI: 10.22541/au.160157552.22382812 (cit. on p. 7).

[24] N. A. Clark, R. H. Wynne and D. Schmoldt, "A review of past research on dendrometers," *Forest Science*, vol. 46, no. 4, pp. 570–576, 2000. DOI: 10.1093/forestscience/46.4.570 (cit. on p. 7).

[25] S. Burgess, M. Adams, N. Turner *et al.*, "An improved heat pulse method to measure low and reverse rates of sap flow in woody plants," *Tree Physiology*, vol. 21, pp. 589–598, 2001. DOI: 10.1093/treephys/21.9.589 (cit. on p. 7).

[26] J. Mendes, D. Gallipoli, A. Tarantino and D. Toll, "On the development of an ultra-high-capacity tensiometer capable of measuring water tensions to 7 mpa," *Géotechnique*, vol. 69, pp. 560–564, 2018. DOI: 10.1680/jgeot.18.t.008 (cit. on p. 7).

[27] W. Whalley, E. Ober and M. Jenkins, "Measurement of the matric potential of soil water in the rhizosphere," *Journal of Experimental Botany*, vol. 64, no. 13, pp. 3951–3963, 2013. DOI: 10.1093/jxb/ert044 (cit. on p. 7).

[28] V. Blanco and L. Kalcsits, "Microtensiometers accurately measure stem water potential in woody perennials," *Plants*, vol. 10, p. 2780, 2021. DOI: 10.3390/plants10122780 (cit. on p. 7).

[29] H. He, N. Turner, G. Ao *et al.*, "Time and frequency domain reflectometry for the measurement of tree stem water content: A review, evaluation, and future perspectives," *Agricultural and Forest Meteorology*, vol. 306, p. 108 442, 2021. DOI: 10.1016/j.agrformet.2021.108442 (cit. on p. 7).

[30] G. Torgovnikov, *Dielectric Properties of Wood and Wood-Based Materials*. 1993. DOI: 10.1007/978-3-642-77453-9 (cit. on p. 7).

[31] R. Allan, L. Pereira and M. Smith, *Crop evapotranspiration-Guidelines for computing crop water requirements-FAO Irrigation and drainage paper 56*. 1998, vol. 56 (cit. on p. 7).

[32] M. Peichl, M. Nilsson, P. Smith *et al.*, *ETC L2 ARCHIVE, Svartberget, 2019-01-01–2024-09-01*, 2024. [Online]. Available: https://hdl.handle.net/11676/aji8KUPQYA4MeDyJBWRnRx0S (cit. on pp. 7, 10).

[33] J. Gutierrez Lopez, Personal communication with Jose Gutierrez Lopez, Department of Forest Ecology and Management, Swedish University of Agricultural Sciences, 2024 (cit. on p. 7).

[34] H. Chu, X. Luo, Z. Ouyang *et al.*, "Representativeness of eddy-covariance flux footprints for areas surrounding AmeriFlux sites," *Agricultural and Forest Meteorology*, vol. 301-302, p. 108 350, 2021. DOI: https://doi.org/10.1016/j.agrformet.2021.108350 (cit. on p. 8).

[35] D. Kool, N. Agam, N. Lazarovitch, J. Heitman, T. Sauer and A. Ben-Gal, "A review of approaches for evapotranspiration partitioning," *Agricultural and Forest Meteorology*, vol. 184, pp. 56–70, 2014. DOI: 10.1016/j.agrformet.2013.09.003 (cit. on p. 8).

[36] M. Anderson, W. Kustas and J. Norman, "Upscaling and downscaling - a regional view of the soil-plant-atmosphere continuum," *Agronomy Journal*, vol. 95, 2003. DOI: 10.2134/agronj2003.1408 (cit. on p. 8).

[37] R. Zweifel, H. Item and R. Häsler, "Link between diurnal stem radius changes and tree water relations," *Tree Physiology*, vol. 21, no. 12-13, pp. 869–877, 2001. DOI: 10.1093/treephys/21.12-13.869 (cit. on p. 8).

[38] R. Zweifel, K. Steppe and F. J. Sterck, "Stomatal regulation by microclimate and tree water relations: Interpreting ecophysiological field data with a hydraulic plant model," *Journal of Experimental Botany*, vol. 58, no. 8, pp. 2113–2131, 2007. DOI: 10.1093/jxb/erm050 (cit. on pp. 8, 10).

[39] K. Steppe, D. Pauw and T. Doody, "A comparison of sap flux density using thermal dissipation, heat pulse velocity and heat field deformation methods," *Agricultural and Forest Meteorology*, vol. 150, pp. 1046–1056, 2010. DOI: 10.1016/j.agrformet.2010.04.004 (cit. on p. 8).

[40] K. Scipal, M. Arcioni, J. Chave *et al.*, "The BIOMASS mission — an ESA Earth Explorer candidate to measure the BIOMASS of the Earth's forests," in *2010 IEEE International Geoscience and Remote Sensing Symposium (IGARSS), Vancouver, Canada*, 2010, pp. 52–55. DOI: 10.1109/IGARSS.2010.5648979 (cit. on pp. 11, 13, 14).

[41] K. McDonald, E. Podest, N. Steiner *et al.*, "NISAR: Seeing beyond the trees to understand wetlands, forests and biodiversity," in *2024 IEEE International Geoscience and Remote Sensing Symposium (IGARSS), Athens, Greece*, 2024, pp. 6775–6778. DOI: 10.1109/IGARSS53475.2024.10641478 (cit. on pp. 11, 13, 14).

[42] M. A. Wulder, T. R. Loveland, D. P. Roy *et al.*, "Current status of Landsat program, science, and applications," *Remote Sensing of Environment*, vol. 225, pp. 127–147, 2019. DOI: 10.1016/j.rse.2019.02.015 (cit. on pp. 11, 13).

[43] D. Petrolati, N. Gebert, D. Geudtner *et al.*, "An overview of the Copernicus Rose-L SAR instrument," in *2023 IEEE International Geoscience and Remote Sensing Symposium (IGARSS), Pasadena, California, USA*, 2023, pp. 4310–4313. DOI: 10.1109/IGARSS52108.2023.10281670 (cit. on pp. 11, 13, 14).

[44] F. Spoto, O. Sy, P. Laberinti *et al.*, "Overview of Sentinel-2," in *2012 IEEE International Geoscience and Remote Sensing Symposium (IGARSS), Munich, Germany*, 2012, pp. 1707–1710. DOI: 10.1109/IGARSS.2012.6351195 (cit. on pp. 11, 13).

[45] R. Torres, I. Navas-Traver, D. Bibby *et al.*, "Sentinel-1 SAR system and mission," in *2017 IEEE Radar Conference (RadarConf)*, 2017, pp. 1582–1585. DOI: 10.1109/RADAR.2017.7944460 (cit. on pp. 11, 13, 14).

[46] D. Schimel, F. D. Schneider and JPL Carbon and Ecosystem Participants, "Flux towers in the sky: Global ecology from space," *New Phytologist*, vol. 224, no. 2, pp. 570–584, 2019. DOI: 10.1111/nph.15934 (cit. on pp. 11, 13).

[47] C. Oliver and S. Quegan, "Understanding synthetic aperture radar images," 2004 (cit. on p. 13).

[48] Y. Okada, S. Nakamura, K. Iribe *et al.*, "System design of wide swath, high resolution, full polarimietoric L-band SAR onboard ALOS-2," in *International Geoscience and Remote Sensing Symposium (IGARSS), Melbourne, VIC, Australia*, 2013, pp. 2408–2411. DOI: 10.1109/IGARSS.2013.6723305 (cit. on p. 13).

[49] S. H. Miura, Y. Kankaku, T. Motohka, Y. Arikawa and S. Suzuki, "ALOS-4/PALSAR-3 current status," in *Sensors, Systems, and Next-Generation Satellites XXVI*, S. R. Babu, A. Hélière and T. Kimura, Eds., International Society for Optics and Photonics, vol. 12264, SPIE, 2022, p. 1 226 407. DOI: 10.1117/12.2636088 (cit. on p. 13).

[50] D. Giudici, A. Monti Guarnieri and J. P. Cuesta Gonzalez, "Pre-flight SAOCOM-1A SAR performance assessment by outdoor campaign," *Remote Sensing*, vol. 9, no. 7, 2017. DOI: 10.3390/rs9070729 (cit. on pp. 13, 14).

[51] A. Araza, S. de Bruin, M. Herold *et al.*, "A comprehensive framework for assessing the accuracy and uncertainty of global above-ground biomass maps," *Remote Sensing of Environment*, vol. 272, p. 112 917, 2022. DOI: https://doi.org/10.1016/j.rse.2022.112917 (cit. on pp. 13, 14).

[52] A. Hillman, P. Rolland, M. Chabot, R. Périard, P. Ledantec and N. Martens, "RADARSAT-2 mission operations status," in *2011 IEEE International Geoscience and Remote Sensing Symposium*, 2011, pp. 3480–3483. DOI: 10.1109/IGARSS.2012.6350449 (cit. on pp. 13, 14).

[53] J. Janoth, S. Gantert, W. Koppe, A. Kaptein and C. Fischer, "TerraSAR-X2 - Mission overview," in *2012 IEEE International Geoscience and Remote Sensing Symposium (IGARSS), Munich, Germany*, 2012, pp. 217–220. DOI: 10.1109/IGARSS.2012.6351599 (cit. on pp. 13, 14).

[54] F. Banda, N. Petrushevsky, S. Tebaldini and A. Monti-Guarnieri, "Space-borne L-band forest TomoSAR: A first case study," in *2024 IEEE International Geoscience and Remote Sensing Symposium, (IGARSS), Athens, Greece*, 2024, pp. 10 885–10 888. DOI: 10.1109/IGARSS53475.2024.10641552 (cit. on p. 14).

[55] O. Csillik, J. Reiche, V. De Sy, A. Araza and M. Herold, "Rapid remote monitoring reveals spatial and temporal hotspots of carbon loss in Africa's rainforests," *Communications Earth Environment*, vol. 3, p. 48, 2022. DOI: 10.1038/s43247-022-00383-z (cit. on p. 14).

[56] M. Dabboor, I. Olthof, M. Mahdianpari *et al.*, "Results update on the performance of the Radarsat Constellation Mission," in *2022 IEEE International Geoscience and Remote Sensing Symposium (IGARSS), Kuala Lumpur, Malaysia*, 2022, pp. 4427–4430. DOI: 10.1109/IGARSS46834.2022.9883906 (cit. on p. 14).

[57] V. Ignatenko, P. Laurila, A. Radius, L. Lamentowski, O. Antropov and D. Muff, "ICEYE microsatellite SAR constellation status update: Evaluation of first commercial imaging modes," in *2020 IEEE International Geoscience and Remote Sensing Symposium (IGARSS), Waikoloa, HI, USA*, 2020, pp. 3581–3584. DOI: 10.1109/IGARSS39084.2020.9324531 (cit. on p. 14).

[58] C. Stringham, G. Farquharson, D. Castelletti *et al.*, "The Capella X-band SAR constellation for rapid imaging," in *2019 IEEE International Geoscience and Remote Sensing Symposium*, 2019, pp. 9248–9251. DOI: 10.1109/IGARSS.2019.8900410 (cit. on p. 14).

[59] *Umbra SAR Constellation*, Accessed: 2024-04-03. [Online]. Available: https://www.eoportal.org/satellite-missions/umbra-sar (cit. on p. 14).

[60] C. Albinet, P. Borderies, T. Koleck *et al.*, "TropiSCAT: A ground based polarimetric scatterometer experiment in tropical forests," *IEEE Journal of Selected Topics in Applied Earth Observations and Remote Sensing*, vol. 5, no. 3, pp. 1060–1066, 2012. DOI: 10.1109/JSTARS.2012.2201917 (cit. on p. 15).

[61] C. Albinet, T. Koleck, T. Le Toan *et al.*, "First results of AfriScat, a tower-based radar experiment in African forest," in *2015 IEEE International Geoscience and Remote Sensing Symposium (IGARSS), Milan, Italy*, 2015, pp. 5356–5358. DOI: 10.1109/IGARSS.2015.7327045 (cit. on p. 15).

[62] S. E. I. Essebtey, L. Villard, P. Borderies, T. Koleck, B. Burban and T. L. Toan, "Comparative study of temporal decorrelation at P, L and C-bands: First insights from the TropiScat-2 experiment," in *2020 Mediterranean and Middle-East Geoscience and Remote Sensing Symposium (M2GARSS)*, 2020, pp. 246–249. DOI: 10.1109/M2GARSS47143.2020.9105253 (cit. on p. 15).

[63] J. Jorge Ruiz, R. Vehmas, J. Lemmetyinen *et al.*, "SodSAR: A tower-based 1–10 GHz SAR system for snow, soil and vegetation studies," *Sensors*, vol. 20, 2020. DOI: 10.3390/s20226702 (cit. on p. 15).

[64] L. M. H. Ulander, A. R. Monteith, H. J. Persson and J. E. S. Fransson, "Borealscat-2: Backscatter measurements of forest water dynamics," in *2024 IEEE International Geoscience and Remote Sensing Symposium (IGARSS), Athens, Greece*, 2024, pp. 2332–2335. DOI: 10.1109/IGARSS53475.2024.10642923 (cit. on p. 16).

[65] F. Ulaby and D. Long, *Microwave Radar and Radiometric Remote Sensing*. Ann Arbor, Michigan: University of Michigan Press, 2014 (cit. on pp. 16, 17).

[66] E. P. Attema and F. T. Ulaby, "Vegetation modeled as a water cloud," *Radio Science*, vol. 13, pp. 357–364, 2 1978. DOI: 10.1029/RS013i002p00357 (cit. on pp. 18, 22).

[67] M. Kurum, S.-B. Kim, R. Akbar and M. H. Cosh, "Surface soil moisture retrievals under forest canopy for L-band SAR observations across a wide range of incidence angles by inverting a physical scattering model," *IEEE Journal of Selected Topics in Applied Earth Observations and Remote Sensing*, vol. 14, pp. 1741–1753, 2021. DOI: 10.1109/JSTARS.2020.3047883 (cit. on p. 19).

[68] M.-L. Truong-Loi, S. Saatchi and S. Jaruwatanadilok, "Soil moisture estimation under tropical forests using UHF radar polarimetry," *IEEE Transactions on Geoscience and Remote Sensing*, vol. 53, pp. 1718–1727, 2015. DOI: 10.1109/TGRS.2014.2346656 (cit. on pp. 19, 22).

[69] P. Bennet, L. Ulander, M. Mariotti d'Alessandro and S. Tebaldini, "Sensitivity of P- and L-band SAR tomography to above-ground biomass in a hilly temperate forest," *IEEE Transactions on Geoscience and Remote Sensing*, vol. 62, pp. 1–1, 2024. DOI: 10.1109/TGRS.2024.3455790 (cit. on p. 19).

[70] J. Askne, M. Soja and L. Ulander, "Biomass estimation in a boreal forest from TanDEM-X data, lidar DTM, and the interferometric water cloud model-nc-nd license (http:// creativecommons.org/licenses/by-nc-nd/4.0/)," *Remote Sensing of Environment*, vol. 196, pp. 265–278, 2017. DOI: 10.1016/j.rse.2017.05.010 (cit. on p. 22).

[71] M. Soja, S. Quegan, M. Mariotti d'Alessandro *et al.*, "Mapping above-ground biomass in tropical forests with ground-cancelled P-band SAR and limited reference data," *Remote Sensing of Environment*, vol. 253, 2020. DOI: 10.1016/j.rse.2020.112153 (cit. on p. 22).

[72] M. Santoro, O. Cartus, S. Quegan *et al.*, "Design and performance of the climate change initiative biomass global retrieval algorithm," *Science of Remote Sensing*, vol. 10, p. 100 169, 2024. DOI: 10.1016/j.srs.2024.100169 (cit. on p. 22).

[73] S. Saatchi and M. Moghaddam, "Estimation of crown and stem water content and biomass of boreal forest using polarimetric SAR imagery," *IEEE Transactions on Geoscience and Remote Sensing*, vol. 38, no. 2, pp. 697–709, 2000. DOI: 10.1109/36.841999 (cit. on p. 22).